

***In situ* observation of the effect of AlN particles on bainitic transformation in a carbide-free medium carbon steel**

Xiao-jie Zhao, Zhi-nan Yang, and Fu-cheng Zhang

Cite this article as:

Xiao-jie Zhao, Zhi-nan Yang, and Fu-cheng Zhang, *In situ* observation of the effect of AlN particles on bainitic transformation in a carbide-free medium carbon steel, *Int. J. Miner. Metall. Mater.*, 27(2020), No. 5, pp. 620-629. <https://doi.org/10.1007/s12613-019-1911-9>

View the article online at [SpringerLink](#) or [IJMMM Webpage](#).

Articles you may be interested in

Wei Liu, You-hui Jiang, Hui Guo, Yue Zhang, Ai-min Zhao, and Yao Huang, [Mechanical properties and wear resistance of ultrafine bainitic steel under low austempering temperature](#), *Int. J. Miner. Metall. Mater.*, 27(2020), No. 4, pp. 483-493. <https://doi.org/10.1007/s12613-019-1916-4>

Ping-hu Chen, Yun Zhang, Rui-qing Li, Yan-xing Liu, and Song-sheng Zeng, [Influence of carbon-partitioning treatment on the microstructure, mechanical properties and wear resistance of *in situ* VCp-reinforced Fe-matrix composite](#), *Int. J. Miner. Metall. Mater.*, 27(2020), No. 1, pp. 100-111. <https://doi.org/10.1007/s12613-019-1909-3>

Yu Li, Li-hua Zhao, Ya-kun Wang, and Da-qiang Cang, [Effects of Fe₂O₃ on the properties of ceramics from steel slag](#), *Int. J. Miner. Metall. Mater.*, 25(2018), No. 4, pp. 413-419. <https://doi.org/10.1007/s12613-018-1586-7>

Gao-jie Li, Ming-xing Guo, Yu Wang, Cai-hui Zheng, Ji-shan Zhang, and Lin-zhong Zhuang, [Effect of Ni addition on microstructure and mechanical properties of Al-Mg-Si-Cu-Zn alloys with a high Mg/Si ratio](#), *Int. J. Miner. Metall. Mater.*, 26(2019), No. 6, pp. 740-751. <https://doi.org/10.1007/s12613-019-1778-9>

Zi-yi Liu, Yan-ping Bao, Min Wang, Xin Li, and Fan-zheng Zeng, [Austenite grain growth of medium-carbon alloy steel with aluminum additions during heating process](#), *Int. J. Miner. Metall. Mater.*, 26(2019), No. 3, pp. 282-290. <https://doi.org/10.1007/s12613-019-1736-6>



IJMMM WeChat



QQ author group

In situ observation of the effect of AlN particles on bainitic transformation in a carbide-free medium carbon steel

Xiao-jie Zhao¹⁾, Zhi-nan Yang²⁾, and Fu-cheng Zhang¹⁾

1) State Key Laboratory of Metastable Materials Science and Technology, Yanshan University, Qinhuangdao 066004, China

2) National Engineering Research Center for Equipment and Technology of Cold Strip Rolling, Yanshan University, Qinhuangdao 066004, China

(Received: 18 July 2019; revised: 15 September 2019; accepted: 18 September 2019)

Abstract: The bainitic transformation of the steels with different mass fractions of N, ~0.002% and 0.021%, was observed *in situ* by using high-temperature metalloscope. Micrometer- and nanometer-sized aluminum nitride (AlN) particles were found in the steel with 0.021% N. Grain boundaries, the interior of the grains, and AlN particles were used as initial nucleation sites of bainitic ferrite, and bainitic ferrite subunits served as new nucleation sites to induce secondary nucleation. The lengthening rate of bainitic ferrite varied at different nucleation sites, which was controlled by the repeated nucleation and growth of bainitic subunits. The AlN particles not only provided several nucleation sites, but also increased the autocatalytic effect on the transformation, further shortening the incubation period, promoting the bainitic transformation, and refining the bainitic microstructure.

Keywords: bainitic steel; *In situ* observation; phase transformation; aluminum nitride

1. Introduction

Carbide-free bainitic steel has excellent mechanical properties and is of great significance in engineering applications, especially in industry [1–3]. However, its applications are limited by its long isothermal transformation time and preparation period, which have resulted in high economic cost. Generally, adjusting alloying elements is an effective way to solve this problem. One approach is to accelerate bainitic transformation by adding alloying elements that increase the free energy difference ($\gamma \rightarrow \alpha$) and phase transformation driving force of thermodynamics [4–5]. Another method is the appropriate reduction of alloying element content, which tends to be segregated at grain boundaries, inhibits the ferrite nucleus, and accelerates bainitic transformation [6–7]. It is notable that the adjustment of alloy elements should consider not only the phase transformation dynamics, but also the effects of the microstructure and comprehensive mechanical properties. Therefore, a reasonable design of components is the key to solving the long isothermal transformation of nano-bainitic steel; microalloying is an effective method to achieve this design.

Microalloying has attracted considerable attention as a method of generating ferrite by introducing inclusions or pre-

cipitations as heterogeneous nucleation points [8–10]. In the field of materials and metallurgy, microalloying in steels is an advanced technology that introduces a small amount of elements, such as V, Ti, and Nb, to form carbides or nitrides. The main mechanisms include the formation of a thin solute-poor zone around particles, which can promote the nucleation of ferrite. Also, a particular orientation relationship has been observed between nitrides (R_xN) and bainitic ferrite (BF), i.e., $(100)_{R_xN} // (100)_{BF}$, $[010]_{R_xN} // [010]_{BF}$; the nitrides were highly homogenous with ferrite, and had a low interfacial energy with the ferrite and a high interfacial energy with austenite [11–12]. Therefore, microalloyed steel resulting from the introduction of nitrides has been designed to increase the nucleation rate of BF and shorten the incubation period of bainitic transformation. Aluminum nitride (AlN) particles have usually been used to control the recrystallization and refine prior austenite grains [13]. However, the effect of AlN particles on bainite transformation has not been considered previously, probably because of its low volume fraction.

Bainitic transformation is a widely-discussed topic among scholars in China and abroad. The “shear school” holds that bainite nucleates and grows by shearing [14]. In contrast, the “diffusion school” believes that bainitic trans-

Corresponding authors: Zhi-nan Yang E-mail: zhinanyang@ysu.edu.cn; Fu-cheng Zhang E-mail: zfc@ysu.edu.cn

© University of Science and Technology Beijing and Springer-Verlag GmbH Germany, part of Springer Nature 2020

formation is the process of sympathetic nucleation-ledge-wise growth; when the composition of the parent phase and new phase is quite different, bainite nucleation is formed at the interface of the new phase, and growth is thickened by the lateral migration of steps [15]. However, to date, the mechanism of bainitic transformation has not been fully elucidated. The nucleation and growth of bainitic transformation are of great significance, and metallography and thermal expansion tests have been the main methods in the research of bainitic transformation. However, the traditional metallographic method is only able to observe bainitic microstructure under a certain time, and nucleation and growth cannot be directly observed. Thus, an in-depth study of the microstructural evolution during nucleation and growth is necessary to study the influencing mechanism of nitrides on bainitic transformation. In recent years, the high-temperature laser confocal microscope (LSCM) has been used to observe the phase transformation process of steel via an intuitive and continuous *in situ* method [16–18]. The influence of austenitizing temperature, austenite grain size, and quenching isothermal temperature on bainitic transformation can be studied accurately using LSCM [19–21].

In this study, the AlN particles were designed by adding Al and N elements in medium carbon carbide-free bainitic steel to study the dynamics of bainitic transformation and microstructure evolution during bainitic transformation. The study was performed using a Gleeble-3500 thermomechanical simulator and LSCM.

2. Experimental

The variation in the volume fraction of AlN particles with the changing mass fractions of Al and N at a certain temperature was obtained, as shown in Fig. 1. The volume fraction of AlN particle was obtained based on the ideal quality ratio of AlN and the solid solubility product formula of AlN in ferrite, as expressed in equations [22]:

$$\lg \{[Al] \cdot [N]\} = -\frac{7184}{T} + 1.79 \quad (1)$$

$$\{W(Al) - [Al]\} / \{W(N) - [N]\} = 27/14 \quad (2)$$

$$f = \{W(Al) - [Al] + W(N) - [N]\} \cdot d_{Fe} / d_{AlN} \quad (3)$$

where T is the temperature, K; $W(Al)$ and $W(N)$ are the mass fractions of aluminum and nitrogen of the test steel; $[Al]$ and $[N]$ are the contents of solid solution aluminum and nitrogen in the matrix at the temperature T , respectively; f is the volume fraction of AlN; d_{Fe} and d_{AlN} are the densities of Fe

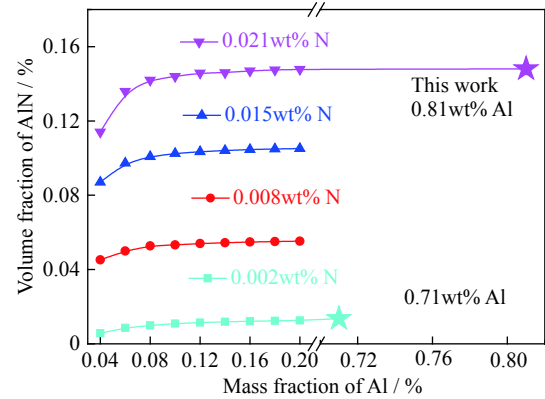


Fig. 1. Curves of volume fraction of AlN with different mass fractions of Al and N at 930°C.

and AlN, which are 7.875 g/cm³ and 3.263 g/cm³, respectively.

According to the equations above, it was determined that, when the mass fraction of N is constant, the volume fraction of AlN particles initially increases gradually with an increase in the mass fraction of Al until a saturation value is achieved. When the mass fraction of Al is fixed, the volume fraction of AlN always increases with increasing the mass fraction of N. Therefore, the volume fraction of AlN in steels is primarily controlled by the mass fraction of N. From these results, two sets of test materials, with different mass fractions of N, were designed. The chemical compositions of the two steels are given in Table 1. On the basis of the mass fraction of N, the two steels are denoted as 20N and 210N. The theoretical volume fractions of AlN particles in the 20N and 210N steels at 930°C were 0.0136% and 0.148%, respectively, based on Eq. (1) and the ideal mass ratio formula of AlN. The volume fraction of AlN particles in the 210N steel was approximately 10 times that in the 20N steel.

The steels were smelted using a vacuum melting furnace and forged with a forging ratio of 6. The two steels were solution-treated at 1300°C for 30 min, cooled to 930°C, held at that temperature for 30 min, and then quenched to ambient air temperature to control nitride particles. The isothermal bainitic transformation was measured via a Gleeble-3500 thermomechanical simulator and the sample with a gage of 10 mm and a gage diameter of 6 mm was fabricated. After solution treatment, the steels were heated to 930°C at a rate of 10°C·s⁻¹, held for 10 min, cooled to 320°C at a rate of 30°C·s⁻¹, and held until bainitic transformation was completed.

The microstructural evolution during bainitic transform-

Table 1. Chemical compositions of the investigated steels

Steel	C	Si	Mn	Cr	Ni	Mo	Al	N
210N	0.34	1.32	1.60	1.20	0.80	0.55	0.81	0.021
20N	0.35	1.48	1.52	1.15	0.93	0.40	0.71	0.002

ation was dynamically observed by LSCM. The sample size for measuring was 3 mm in length and 6 mm in diameter. The top and bottom surfaces of the samples were polished conventionally to keep the measurement surface smooth and minimize the effect of surface roughness. Samples were heated to an austenitization temperature of 930°C at a rate of 100°C·min⁻¹, held for 10 min, and then cooled to 320°C at a rate of 300°C·min⁻¹. Microstructures were examined using SU-5000 scanning electron microscopy and a JEOL-2010 transmission electron microscope (TEM). Samples were then thinned to perforation on a TenuPol-5 twin-jet unit with an electrolyte consisting of 7vol% perchloric acid and 93vol% glacial acetic acid. Morphology and orientation of the bainitic sheaves were characterized by electron-backscattered diffraction microscopy (EBSD). The scanning step length was 0.08 μm and the voltage was 30 kV. X-ray experiments were conducted with a step width of 0.02° and counting time of 2 s over the 2θ range of 20° to 120° with unfiltered Cu K_α. Under the conditions of only body-centered cubic (α) and face-centered cubic (γ) phases, the volume fraction of retained austenite (V_γ) was calculated using Eq. (4) [23]:

$$V_\gamma = \frac{\frac{1}{n} \sum_{j=1}^n \frac{I_\gamma^j}{R_\gamma^j}}{\frac{1}{n} \sum_{j=1}^n \frac{I_\gamma^j}{R_\gamma^j} + \frac{1}{n} \sum_{j=1}^n \frac{I_\alpha^j}{R_\alpha^j}} \quad (4)$$

where n is the number of peaks, I_γ^j and I_α^j are the integrated intensity of the diffraction peak of retained austenite and bainitic ferrite, and R_γ^j and R_α^j are the material scattering factor of retained austenite and bainitic ferrite, respectively.

3. Results

3.1. Transformation kinetics

Fig. 2(a) shows the dilation–time curves of the 20N and 210N steels that underwent isothermal treatment at 320°C. The horizontal gage line of the 20N and 210N steels was maintained at the beginning of the isothermal treatment process. After 1.5 min of incubation, the dilation–time curve of the 210N steel deviated upward from the straight lines with a significant increase in expansion. Meanwhile, after approximately 3 min of incubation, the dilation–time curve of the 20N steel deviated from the lines. This finding directly indicated that the transformation rate of the 210N steel exhibited a more evident increase after a shorter incubation period compared with that of the 20N steel. Moreover, the overall transformation time in the 210N steel (about 20.3 min) is reduced by approximately 24% compared with that in the 20N steel (about 26.7 min). The volume fraction of retained austenite (RA) was estimated on the basis of the X-ray diffraction results shown in Fig. 2(b). When the steels transformed at

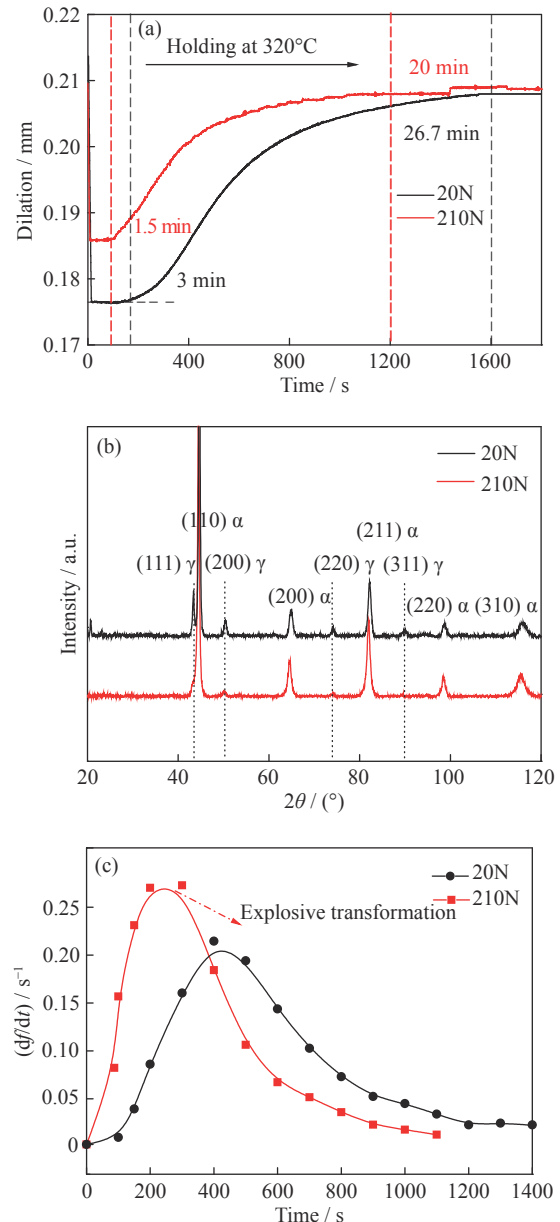


Fig. 2. Isothermal treatment results of the 20N and 210N steels at 320°C: (a) dilation–time curves; (b) XRD patterns; (c) df/dt –time curves.

320°C, the microstructures were carbide-free bainite. The volume fraction of RA was calculated using Eq. (4). The volume fractions of RA were 7.92% ± 0.52% and 3.51% ± 0.79% for the 20N and 210N steels, respectively. The differential equation was obtained by taking the derivatives of the volume fraction of BF (f) [24]:

$$\frac{df}{dt} = (1-f)(1+\lambda f)k \quad (5)$$

where k is the parameter related to the composition and temperature of the sample and λ is the parameter of autocatalytic nucleation, which is related to the variation in the volume fraction of BF with different times during isothermal treat-

ment [25]. The autocatalytic parameter λ increased with increasing curvature of the curve. The df/dt -time curve (Fig. 2(c)) shows that the autocatalytic parameter increased significantly at the early reaction stage when explosive transformation occurred. In summary, these results indicated that the bainitic transformation of 210N steel was expedited and the transformation degree of BF was facilitated. Thus, internal action within the microstructure should be considered in the analysis of accelerated transformation.

3.2. Microstructural characterization

Fig. 3 shows the microstructures of the 20N and 210N steels at 320°C. The microstructures of the 20N and 210N steels consisted of BF plates and filmy and blocky RA. The apparent thickness of BF of 210N steel ranged between 80 and 120 nm, whereas that of the 20N steel ranged between 100 and 140 nm. The true thicknesses of the BF (t_a) and RA (t_r) were calculated using the formula: $t = 2L_T/\pi$, $E = \pm 2\sigma_L/(\pi\sqrt{N})$ [26–27], where L_T is the linear intercept length measured in the TEM images, E is the 95% confidence interval, σ_L is the standard deviation of the true thickness, and N is the number of counted plates. Statistical results indicated that the average thickness of the BF plates was (107 ± 3) nm for the 20N steel and (92 ± 2) nm for the 210N steel. Therefore, the bainitic microstructure of the 210N steel was more refined than that of the 20N steel. Detailed characterizations indicated that particles existed on varying scales. Some micro-sized AlN particles with a radius of approximately 5 μm and a small amount of strip nanosized precipitation with a size of 150 nm \times 40 nm were dispersed within the microstructure of the 210N steel, as shown in Figs. 3(c) and 3(f).

EBSD technique was used to characterize the microstructures of the samples. Orientation images and misorientation angle distributions of these samples based on statistical

analysis are shown in Fig. 4. The 20N and 210N steels transformed at 320°C both exhibited a large proportion of misorientation in the 50°–60° range and a small fraction of low-angle misorientation (<20°). This finding indicated that the bainitic microstructure after isothermal transformation was lower bainite [28]. The 210N steel after isothermal bainitic transformation at 320°C showed a larger proportion of misorientation in the 50°–60° range and a smaller proportion of low-angle misorientation compared with the 20N steel. The results showed that local variations could be produced during bainitic transformation to adapt to the strain from the transformation, and the size of the bainite sheaf was affected by the location of the nucleation sites. Owing to the large number of nucleation sites in the 210N steel, the selection of variants was enhanced and the large angle of the BF increased with many variations. This improvement resulted in the increased misorientation in the 50°–60° range and decreased the size of the BF sheaf.

3.3. *In situ* observation of the nucleation and growth process

In situ observation of the nucleation sites and the growth rates of bainite in 210N and 20N steels via LSCM were carried out. Fig. 5 shows the evolution of the bainitic microstructure. The grain boundaries of prior austenite and nucleation sites were analyzed. The average grain sizes of prior austenite in the 210N and 20N steels were (23 ± 6) μm and (24 ± 5) μm , respectively. The nucleation sites of bainite in the 20N steel were observed. Three main types of nucleation sites were found, i.e., grain boundary, inner grain, and BF boundary (Fig. 5(b)). Nucleation of the 20N steel was preferred at grain boundaries in the early stage. Also, nucleation was induced at the defects within the grain. With increasing isothermal time, the BF boundary was formed as a new nuc-

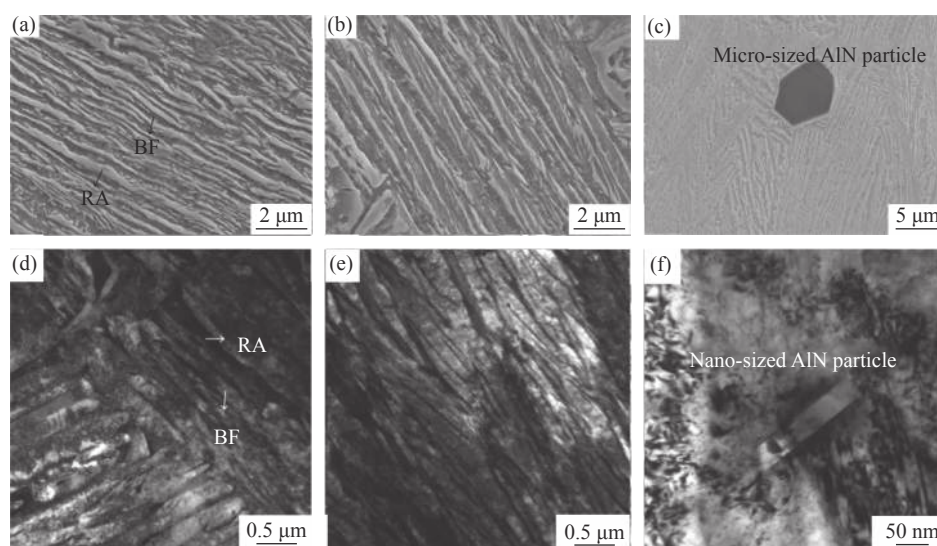


Fig. 3. Microstructures of (a, d) 20N steel and (b, e) 210N steel after isothermal treatment at 320°C, and (c, f) morphologies of AlN particles in 210N steel.

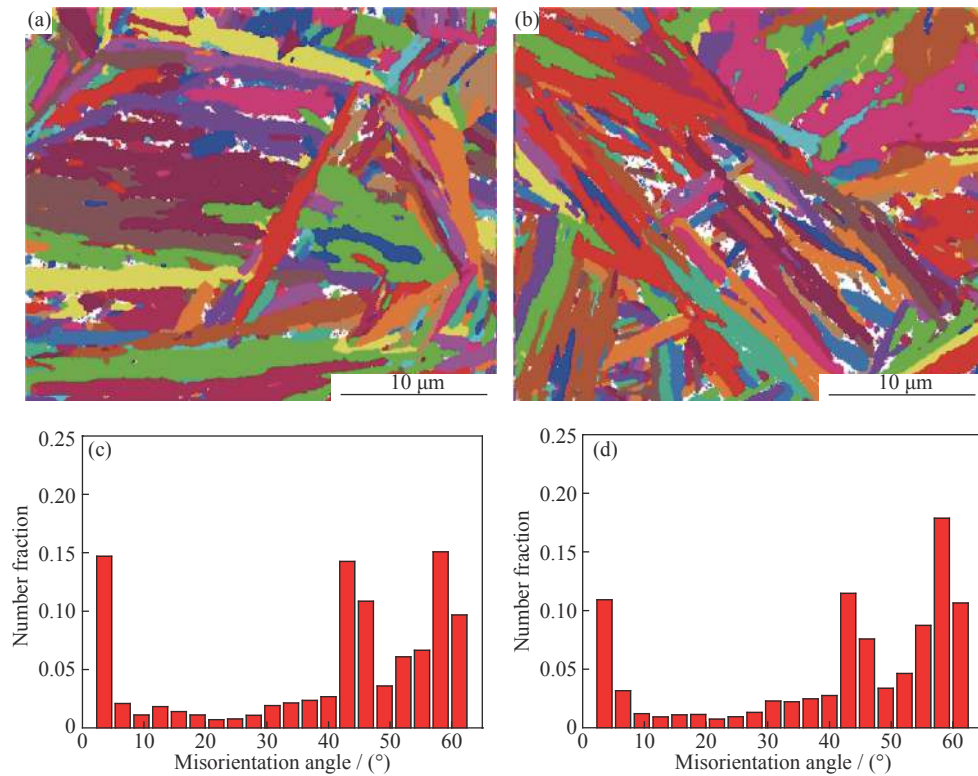


Fig. 4. Orientation images and misorientation angle distributions of (a, c) 20N steel and (b, d) 210N steel transformed at 320°C.

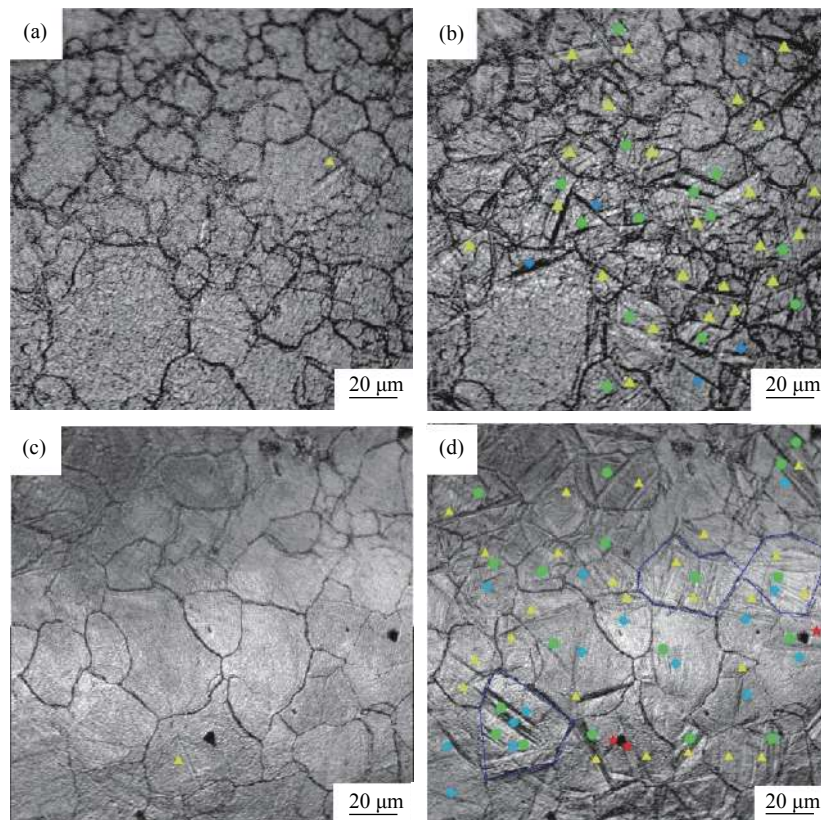


Fig. 5. Nucleation of 20N and 210N steels with different isothermal times: (a) 20N steel, 10 s; (b) 20N steel, 150 s; (c) 210N steel, 10 s; (d) 210N steel, 150 s. ▲ Grain boundary; ● Phase boundary; ◆ Inner grain; ★ AlN particle.

leation site to induce the subsequent formation of the BF. These nucleation sites increased significantly. The nuclei of the 210N steel were also preferred at grain boundaries. Compared with those in the 20N steel, the AlN particles in the 210N steel could serve as nucleation sites (Fig. 5(d)). Generally, there were more nuclei of BF within the grain than at the grain boundary, so that the BF boundaries induced more secondary nucleation. Fig. 6 shows the curves of the number of nuclei with isothermal time in the 20N and 210N steels. The nuclei at the grain boundaries of the two test steels were

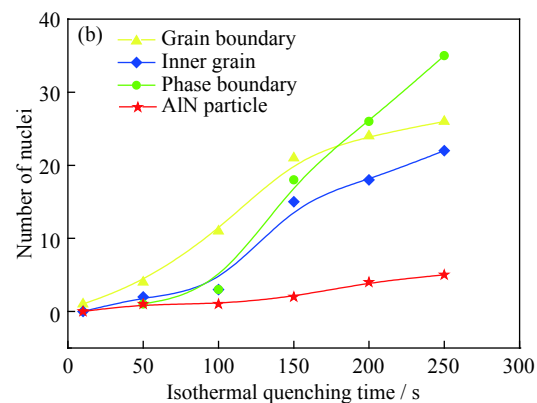
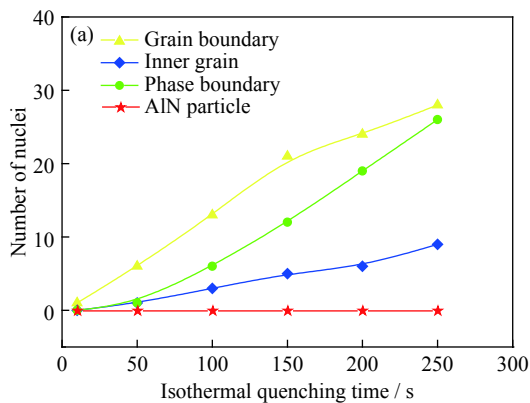


Fig. 6. Curves of the number of nuclei with isothermal time in the (a) 20N and (b) 210N steels.

By comparison, the different nucleation sites of the BF in the 20N and 210N steels also had different growth rates. In addition to elongation, the bainitic microstructure was also coarsened, although the elongation often occurred prior to widening. Through statistical analysis, the lengthening rates of the BF within the grain were $0.54 \mu\text{m/s}$ (Fig. 7) and $0.78 \mu\text{m/s}$ (Fig. 8) in the 20N and 210N steels, respectively, when the isothermal time of bainitic transformation was 50 s. When the isothermal time of bainitic transformation was 90 s, the lengthening rates of the BF at the grain boundaries were $0.36 \mu\text{m/s}$ (Fig. 9) and $0.38 \mu\text{m/s}$ (Fig. 10) in the 20N and 210N steels, respectively. Therefore, the lengthening rates of the BF at the grain boundaries in the two steels were approximately the same but less than the lengthening rate within the grain. At the same time, the lengthening rate of the BF within the grain in the 210N steel was greater than that in the 20N steel. The tip of the initial BF subunit formed new immature subunits, which continued to grow and merge until they attached to the tip of the primitive bainitic embryos or sheaves. The elongation of the BF subunit was hindered when it encountered the prior austenite grain boundaries or BF phase boundaries. The austenite/bainite and bainite/bainite interfaces were defect planes, which were taken as the shear core in the isothermal process, while the widening of the bainite occurred through the movement of the bainite/austenite interface along the defect (twins or stacking faults) planes [18].

The lengthening rate of the bainite was higher than the widening rate because the number of subunits formed at the

dominant at the early stage of isothermal transformation. Moreover, the number of secondary nuclei at the phase boundaries of the 210N steel exceeded the number of nuclei at the grain boundaries at the later stage. At the same time, the overall nucleation rate of the 210N steel was much higher than that of the 20N steel at the later stage. With increasing transformation, the number of nuclei within the grain and phase boundaries of the 210N steel significantly increased, which was closely related to the introduction of AlN particles.

side of BF was less and the stress–strain field of the BF tip was higher than that of the BF side. The more abundant secondary nucleation sites of the 210N steel facilitated the elongation of the bainitic microstructure; hence, its lengthening rate was relatively high. At the same time, due to the higher number of initial nucleation sites in the 210N steel, no clear widening occurred while the growth rate of the bainitic microstructure in the 210N steel was increasing.

4. Discussion

Growth rates of the bainitic plates at different nucleation sites were estimated based on the lengths of the bainitic plates at different times as observed in the LSCM micrographs. Multiple data sets of micrographs were counted and the lengthening rates during the isothermal process were measured, as shown in Table 2. Analysis and calculation showed that the growth rates of the bainitic plates varied with different nucleation sites during the isothermal holding processes. By comparison, the largest average growth rate of the bainitic plates in the two steels both occurred within grains. The average growth rate in the 210N steel at the grain boundaries was about half of that of bainitic plates within grains. This phenomenon was triggered by AlN particles within grains, which provided more nuclei.

The microstructure of the 210N steel showed that micrometer- and nanometer-sized AlN particles were present in the 210N steel. Therefore, the nuclei points within the grain ob-

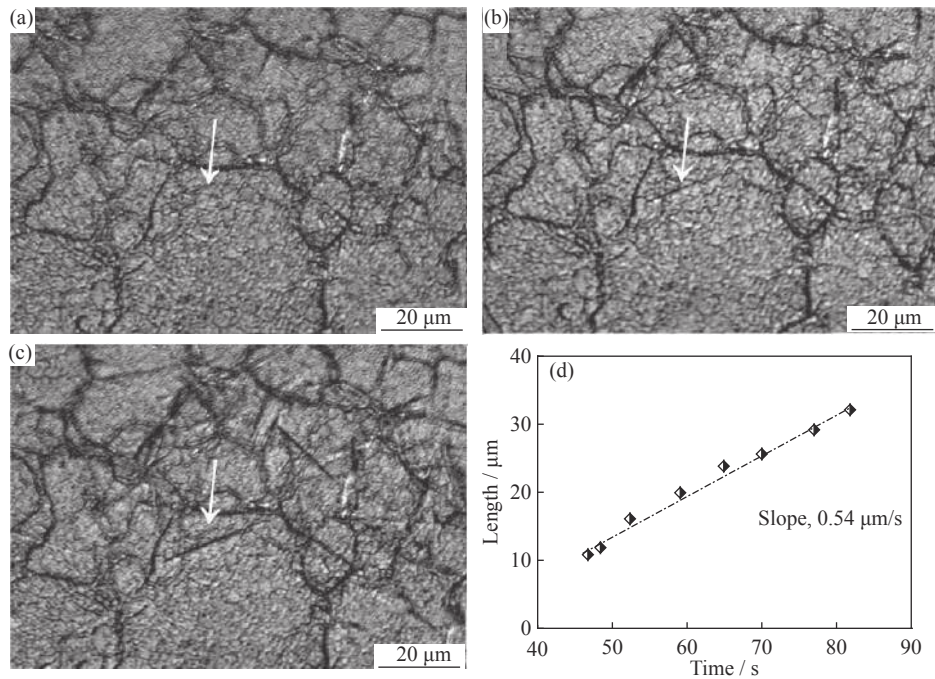


Fig. 7. Micrographs of the lengthening of a bainitic sheaf nucleated within the grain in the 20N steel at different isothermal times: (a) 50 s, (b) 60 s, and (c) 80 s; (d) length–time plot.

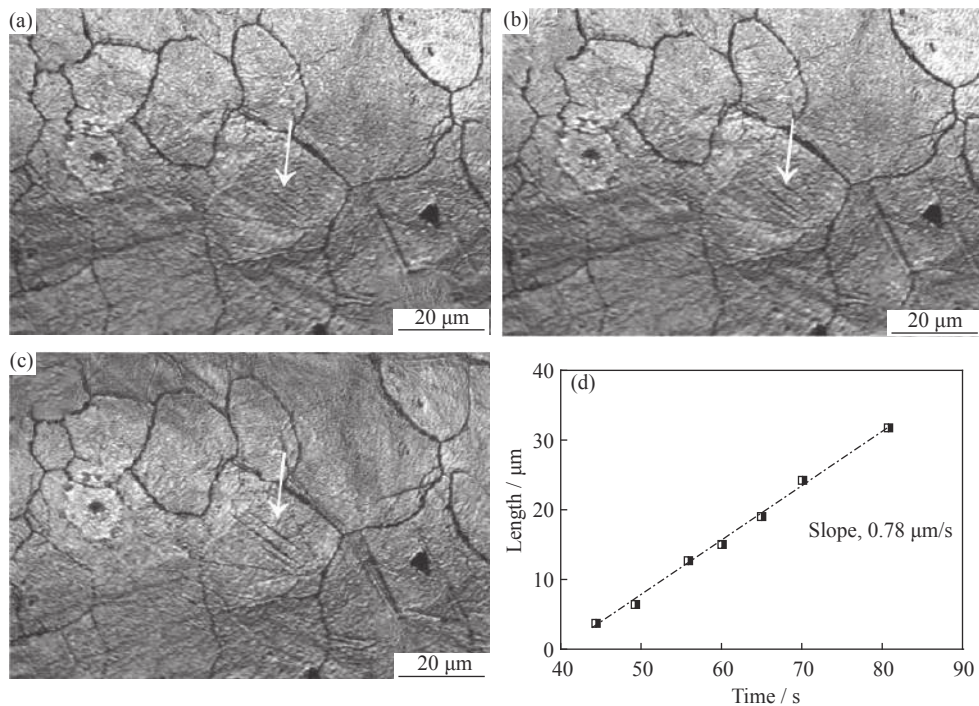


Fig. 8. Micrographs of the lengthening of a bainitic sheaf nucleated within the grain in the 210N steel at different isothermal times: (a) 50 s, (b) 60 s, and (c) 75 s; (d) length–time plot.

served through LSCM not only revealed the existence of defects in the grain, but also were induced by nanosized AlN particles. Two main processes were involved in the formation of bainite nuclei. The first process involved the initial nucleus, which nucleated at the grain boundaries of the prior

austenite, at defects within the grain, and at the boundaries of the AlN particles. The second process involved the autocatalytic nucleus, in which the BF continued to nucleate on the boundaries of the previously-formed lamellar ferrite subunits.

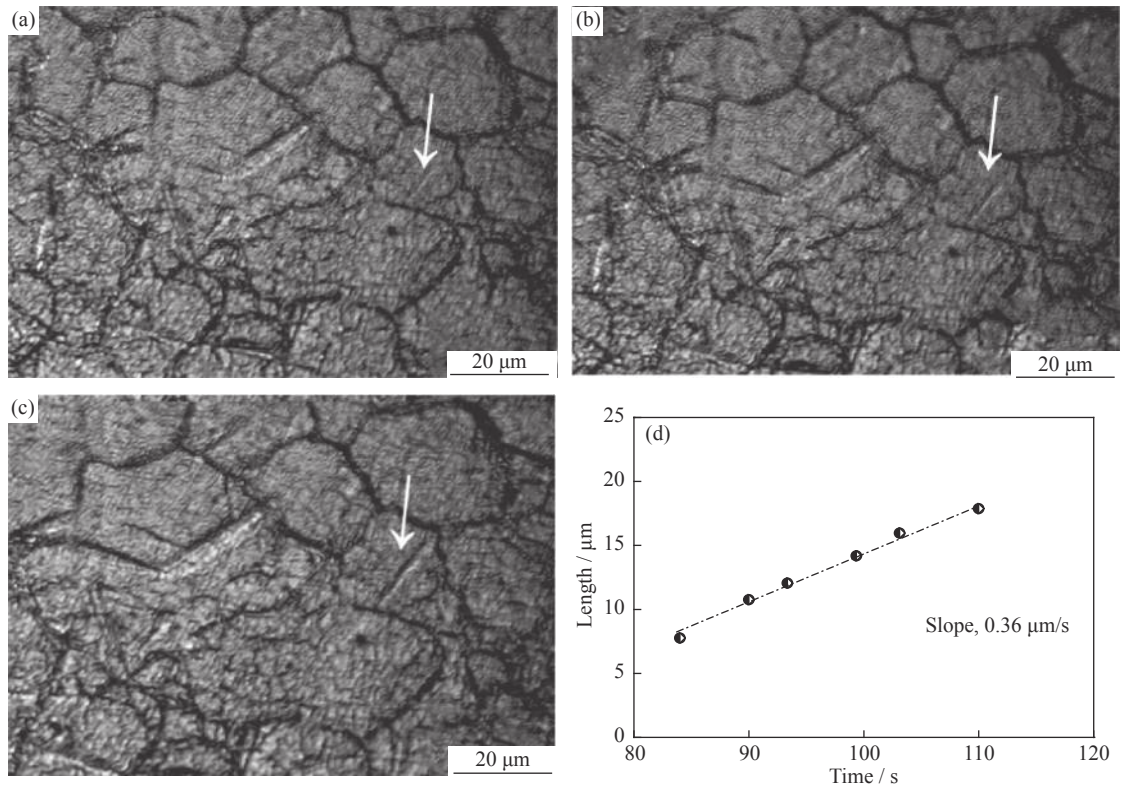


Fig. 9. Micrographs of the lengthening of a bainitic sheaf nucleated at the grain boundaries in the 20N steel at different isothermal times: (a) 90 s, (b) 100 s, and (c) 110 s; (d) length–time plot.

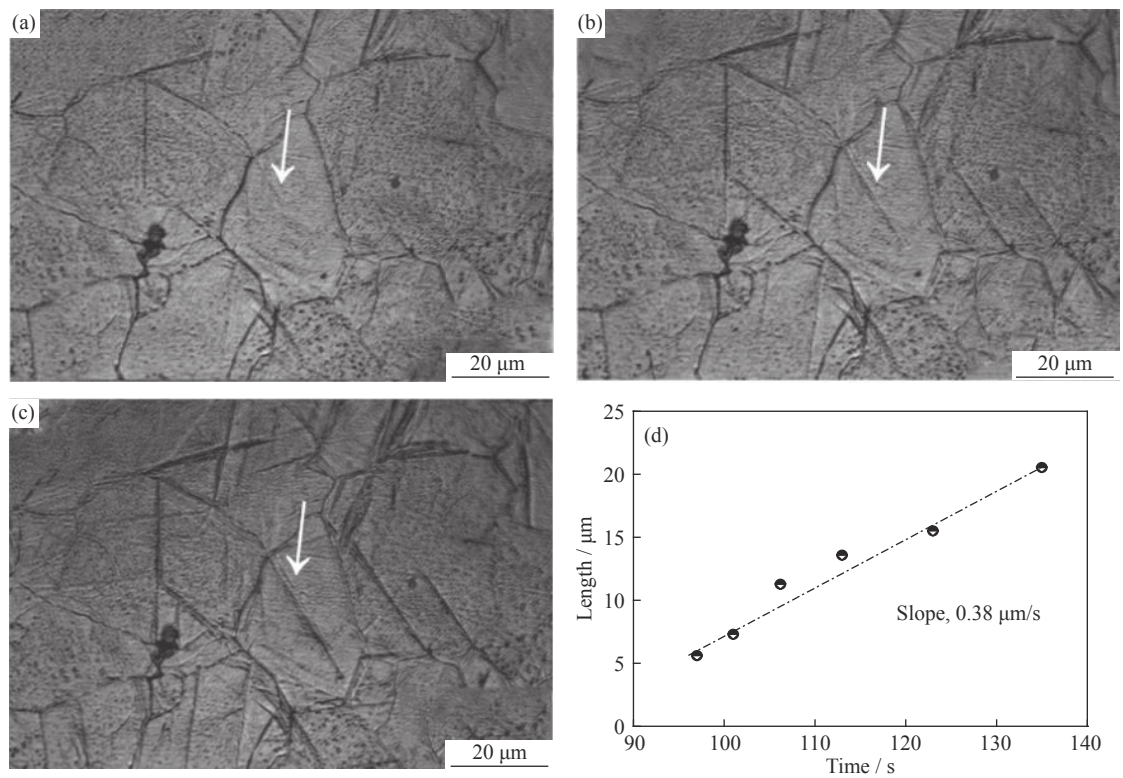


Fig. 10. Micrographs of the lengthening of a bainitic sheaf nucleated at the grain boundaries in the 210N steel at different isothermal times: (a) 90 s, (b) 110 s, and (c) 130 s; (d) length–time plot.

Based on these results, a schematic description of the nucleation and growth of BF on the 210N steel is shown in Fig. 11. BF initially nucleated at positions a, b, and c after the incubation period (position a is the nucleation site provided by the grain boundary of the prior austenite, position b is the nucleation site provided by the defects within the grain, and position c is the nucleation site provided by the AlN particles). Compared with conventional nucleation, the BF subunits formed at position c were accompanied by several phase boundaries, such as AlN/ γ and AlN/ α , and the high

strain energy induced by the phase transformation had a strong autocatalytic effect on the subsequent nucleation of the BF [29]. These effects led to spontaneous nucleation of the BF at position c' in a relatively short period of time. Meanwhile, the repeated nucleation of the lamellar subunit at positions a', b', and c' induced BF sheaf growth [30], and bainitic transformation was constantly propagated by the intermittent nucleation of the subunits. These results indicate that the transformation rate of bainite mainly depends on the nucleation rate of bainite [31].

Table 2. Lengthening rates of bainitic plates calculated by *in situ* observation

Nucleation site	20N		210N	
	Number of plates	Lengthening rate / ($\mu\text{m}\cdot\text{s}^{-1}$)	Number of plates	Lengthening rate / ($\mu\text{m}\cdot\text{s}^{-1}$)
Grain boundaries	12	0.29 ± 0.15	12	0.34 ± 0.14
Inner grain	10	0.54 ± 0.26	10	0.71 ± 0.29
Phase boundaries	11	0.37 ± 0.31	11	0.41 ± 0.24
AlN particles	—	—	2	0.19 ± 0.10

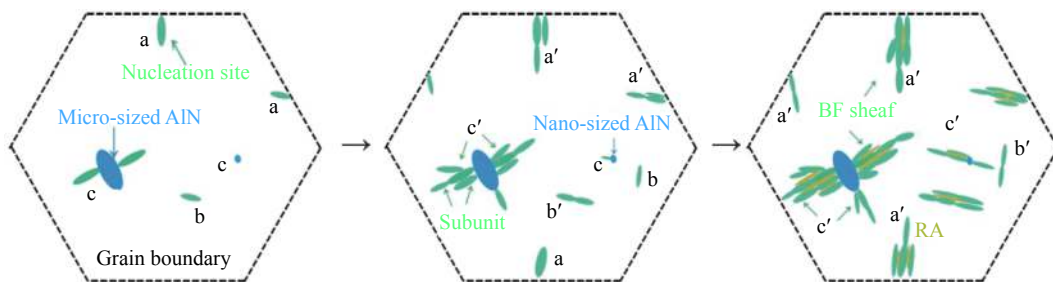


Fig. 11. Schematic description of the nucleation and growth of BF on the 210N steel (positions a, b, and c: initial nucleus; positions a', b', and c': subsequent nucleus).

The lattice misfit between AlN particles and the BF is considered low at 3.6% [32]. The heterogeneous nucleation of the BF induced by the second phase of AlN is inferred to be the main reason for the accelerated bainitic transformation. In conclusion, a certain number of AlN particles in the steels served as catalysts for the bainitic transformation. The particles not only provided multiple nucleation sites, but also increased the autocatalytic effect on the transformation. Moreover, the different thermal expansion coefficients between AlN and prior austenite induced a stress-strain field around the particles, provided extra activation energy for bainite nucleation, and stimulated the nucleation process. Therefore, introducing AlN particles undoubtedly increased the lengthening rate of the BF sheaves, which were nucleated within the grain and accelerated bainitic transformation. This finding is the primary reason for the shorter transformation time of the 210N steel compared to the 20N steel. Furthermore, a large number of BF nuclei in the 210N steel directly resulted in a refined microstructure.

5. Conclusions

The present study explains the effect of AlN particles on

bainitic transformation in a microalloying bainitic steel. Combining transformation kinetics with *in situ* observation of the nucleation and growth, our conclusions are as follows.

(1) The nucleation and growth of BF in medium carbon steel are observed *in situ* using a high-temperature metallography. Grain boundaries are dominant in the nuclei positions at the early stage of bainitic transformation in 20N and 210N steels. However, the subsequent nucleation at the boundaries of BF in the 210N steel plays a leading role in the nucleation process with increasing isothermal time.

(2) Micrometer- and nanometer-sized AlN particles were found in the 210N steel. The low lattice misfit between the BF and AlN particles made the particles the initial nucleation points that induced bainitic transformation. A large number of initial nuclei, which can automatically promote subsequent nucleation, shortened the incubation period in 210N steel.

(3) Growth rates of BF at different nuclei positions vary. The rates are controlled by the repeated nucleation and growth of bainitic subunits. The existence of AlN particles in the 210N steel resulted in the rapid growth of BF nucleated within the grain.

Acknowledgements

This work was financially supported by the Research Project of Hebei Provincial Department of Education (No. QN2018144) and the National Natural Science Foundation of China (No. 51831008).

References

- [1] M. Zhang, T.S. Wang, Y.H. Wang, J. Yang, and F.C. Zhang, Preparation of nanostructured bainite in medium-carbon alloy steel, *Mater. Sci. Eng. A*, 568(2013), p. 123.
- [2] J. Yang, T.S. Wang, B. Zhang, and F.C. Zhang, High-cycle bending fatigue behavior of nanostructured bainitic steel, *Scripta Mater.*, 66(2012), No. 6, p. 363.
- [3] W. Solano-Alvarez, E.J. Pickering, and H.K.D.H. Bhadeshia, Degradation of nanostructured bainitic steel under rolling contact fatigue, *Mater. Sci. Eng. A*, 617(2014), p. 156.
- [4] C. Garcia-Mateo, F.G. Caballero, and H.K.D.H. Bhadeshia, Acceleration of low-temperature bainite, *ISIJ Int.*, 43(2003), No. 11, p. 1821.
- [5] M. Soliman and H. Palkowski, Development of the low temperature bainite, *Arch. Civ. Mech. Eng.*, 16(2016), No. 3, p. 403.
- [6] H. Huang, M.Y. Sherif, and P.E.J. Rivera-Díaz-del-Castillo, Combinatorial optimization of carbide-free bainitic nanostructures, *Acta Mater.*, 61(2013), No. 5, p. 1639.
- [7] T. Sourmail and V. Smanio, Low temperature kinetics of bainite formation in high carbon steels, *Acta Mater.*, 61(2013), No. 7, p. 2639.
- [8] M. Enomoto, Nucleation of phase transformations at intragranular inclusions in steel, *Met. Mater.*, 4(1998), No. 2, p. 115.
- [9] S.D. Catteau, H.P. Van Landeghem, J. Teixeira, J. Dulcy, M. Dehmas, S. Denis, A. Redjaïmia, and M. Courteaux, Carbon and nitrogen effects on microstructure and kinetics associated with bainitic transformation in a low-alloyed steel, *J. Alloys Compd.*, 658(2016), p. 832.
- [10] Y. Luo, W. Yang, Q. Ren, Z.Y. Hu, M. Li, and L.F. Zhang, Evolution of non-metallic inclusions and precipitates in oriented silicon steel, *Metall. Mater. Trans. B*, 49(2018), No. 3, p. 926.
- [11] S.F. Medina, M. Gómez, and L. Rancel, Grain refinement by intragranular nucleation of ferrite in a high nitrogen content vanadium microalloyed steel, *Scripta Mater.*, 58(2008), No. 2, p. 1110.
- [12] M. Sennour and C. Esnouf, Contribution of advanced microscopy techniques to nano-precipitates characterization: case of AlN precipitation in low-carbon steel, *Acta Mater.*, 51(2003), No. 4, p. 943.
- [13] N.E.V. Díaz, S.S. Hosmani, R.E. Schacherl, and E.J. Mittemeijer, Nitride precipitation and coarsening in Fe–2.23 at.% V alloys: XRD and (HR)TEM study of coherent and incoherent diffraction effects caused by misfitting nitride precipitates in a ferrite matrix, *Acta Mater.*, 56(2008), No. 16, p. 4137.
- [14] J. Yang, T.S. Wang, B. Zhang, and F.C. Zhang, Microstructure and mechanical properties of high-carbon Si–Al-rich steel by low-temperature austempering, *Mater. Des.*, 35(2012), p. 170.
- [15] C.Y. Zhang, Q.F. Wang, J.X. Ren, R.X. Li, M.Z. Wang, F.C. Zhang, and Z.S. Yan, Effect of microstructure on the strength of 25CrMo48V martensitic steel tempered at different temperature and time, *Mater. Des.*, 36(2012), p. 220.
- [16] D. Zhang, H. Terasaki, and Y.I. Komizo, *In situ* observation of phase transformation in Fe–0.15C binary alloy, *J. Alloys Compd.*, 484(2009), No. 1-2, p. 929.
- [17] J.W. Elmer, J. Wong, and T. Ressler, *In-situ* observations of phase transformations during solidification and cooling of austenitic stainless steel welds using time-resolved X-ray diffraction, *Scripta Mater.*, 43(2000), p. 751.
- [18] M.K. Kang, M.X. Zhang, and M. Zhu, *In situ* observation of bainite growth during isothermal holding, *Acta Mater.*, 54(2006), No. 8, p. 2121.
- [19] J. Pak, D.W. Suh, and H.K.D.H. Bhadeshia, Displacive phase transformation and surface effects associated with confocal laser scanning microscopy, *Metall. Mater. Trans. A*, 43(2012), No. 12, p. 4520.
- [20] G. Xu, F. Liu, L. Wang, and H.J. Hu, A new approach to quantitative analysis of bainitic transformation in a superbainite steel, *Scripta Mater.*, 68(2013), No. 11, p. 833.
- [21] J. Tian, G. Xu, L. Wang, M.X. Zhou, and H.J. Hu, *In situ* observation of the lengthening rate of bainite sheaves during continuous cooling process in a Fe–C–Mn–Si superbainitic steel, *Trans. Indian Inst. Met.*, 71(2018), No. 1, p. 185.
- [22] Y. Wan, W.Q. Chen, and S.J. Wu, Effect of the hot charging temperature of slabs on AlN and MnS precipitation behavior in non-oriented silicon steel, *J. Univ. Sci. Technol. Beijing*, 35(2014), No. 8, p. 1007.
- [23] A.K. De, D.C. Murdock, M.C. Mataya, J.G. Speer, and D.K. Matlock, Quantitative measurement of deformation-induced martensite in 304 stainless steel by X-ray diffraction, *Scripta Mater.*, 50(2004), No. 12, p. 1445.
- [24] S.M.C.V. Bohemen and J. Sietsma, The kinetics of bainite and martensite formation in steels during cooling, *Mater. Sci. Eng. A*, 527(2010), No. 24-25, p. 6672.
- [25] A.M. Ravi, J. Sietsma, and M.J. Santofimia, Bainite formation kinetics in steels and the dynamic nature of the autocatalytic nucleation process, *Scripta Mater.*, 140(2017), p. 82.
- [26] J. Kang, F.C. Zhang, X.W. Yang, B. Lv, and K.M. Wu, Effect of tempering on the microstructure and mechanical properties of a medium carbon bainitic steel, *Mater. Sci. Eng. A*, 686(2017), p. 150.
- [27] L.C. Chang and H.K.D.H. Bhadeshia, Austenite films in bainitic microstructures, *Mater. Sci. Technol.*, 11(1995), No. 9, p. 874.
- [28] S. Zajac, V. Schwinn, and K.H. Tacke, Characterisation and quantification of complex bainitic microstructures in high and ultra-high strength linepipe steels, *Mater. Sci. Forum*, 500-501(2005), p. 387.
- [29] R.T.V. Tol, L. Zhao, and J. Sietsma, Kinetics of austenite decomposition in manganese-based steel, *Acta Mater.*, 64(2014), p. 33.
- [30] H.K.D.H. Bhadeshia, Bainite: Overall transformation kinetics, *J. Phys. Colloq.*, 43(1982), p. C4443.
- [31] A.M. Ravi, J. Sietsma, and M.J. Santofimia, Exploring bainite formation kinetics distinguishing grain-boundary and autocatalytic nucleation in high and low-Si steels, *Acta Mater.*, 105(2016), p. 155.
- [32] X.J. Zhao, Z.N. Yang, F.C. Zhang, X.Y. Long, and C. Chen, Acceleration of bainitic transformation by introducing AlN in medium carbon steel, *Mater. Sci. Technol.*, 35(2019), No. 2, p. 147.